Shiga toxin-targeted gold nanorods for head-neck cancer photothermal therapy in clinical samples

Elena Navarro-Palomares
University of Cantabria
Lorena García-Hevia
University of Cantabria
Jesús Galán-Vidal
Valdecilla Health Research Institute IDIVAL
Alberto Gandarillas
Valdecilla Health Research Institute IDIVAL
Fe García-Reija
Valdecilla Hospital HUVM
Ana Sánchez-Iglesias
CIC biomaGUNE, Basque Research and Technology Alliance (BRTA), Biomateriales y Nanomedicina (CIBER-BBN)
Luis M. Liz-Marzán
CIC biomaGUNE, Basque Research and Technology Alliance (BRTA), Biomateriales y Nanomedicina (CIBER-BBN)
Rafael Valiente
University of Cantabria
Mónica L. Fanarraga (fanarrag@unican.es)
University of Cantabria

Research Article

Keywords: Functionalized nanomaterial, natural-ligand, nanoparticle targeting, squamous carcinoma, glycosphingolipid, CD77

Posted Date: May 17th, 2022

DOI: https://doi.org/10.21203/rs.3.rs-1640813/v1

Abstract

Background A great challenge in nanomedicine, and more specifically in theranostics, is to improve the specificity and selectivity of nanomaterials towards target tissues or cells. The topical use of nanomedicines as adjuvants to systemic chemotherapy can significantly improve the survival of patients affected by localized carcinomas, reducing the side effects of traditional drugs and preventing local recurrences.

Results Here we have used the Shiga toxin, to design a safe, high-affinity protein-ligand (ShTxB) to bind the globotriaosylceramide receptor (GB3) that is overexpressed on the surfaces of preneoplastic and malignant cancer cells in head and neck tumors. We find that ShTxB functionalized gold nanorods are efficiently retrotranslocated to the GB3 positive cell cytoplasms. After 3-10 minutes of laser radiation with a wavelength resonant with the AuNR longitudinal localized surface plasmon, the death of the targeted cancer cells is activated. Both preclinical models and patient biopsy cells show the non-cytotoxic nature of these functionalized nanoparticles prior to light activation and their treatment selectivity.

Conclusions These results show how the topical use of nanomedicines targeted by natural ligands can represent an effective treatment for aggressive localized cancers, such as squamous cell carcinoma of the head and neck.

Introduction

Nanomedicine has ushered in a new era in drug delivery, improving drug stability and targeting, while reducing biodegradation. However, targeting nanomaterials efficiently to tissues and controlling their intracellular fate are among the major issues in nanomedicine, resulting in that low success in the `bench-to-bed´ translation. As with chemotherapy, it is estimated that less than 1% of systemically administered nanomedicines reach the tumor stroma [1–4]. Hence, nanomaterials' low targeting efficiency and potential toxicity are considered a double-edged sword that limit their application.

To improve the specificity, biocompatibility and selectivity of nanomedicines, nanomaterials are functionalized through surface modifications. Most nanotherapies under development are based on the conjugation of nanoparticles with antibodies, or fragments thereof, for their specific targeting to receptors on tumor cells, to which they bind with high affinity. However, nanoparticle instability, the limited penetration into tissues, and the inability to cross cell membranes are the main disadvantages. As a consequence, drug concentrations administered to tumor cells do not reach threshold therapeutic doses, often generating resistance. But, until the targeting of systemically administered nanomaterials improves, nanomedicine could have enormous potential in the local treatment of accessible cancers, especially those that have imprecise borders or cause recurrences of adjacent neoplastic cells.

In this scenario, virus and toxin recognition mechanisms offer an interesting alternative. These natural systems have evolved over millions of years to perfect their targeting, cell entry, and infection mechanisms binding specific receptors with nanomolar affinities [5, 6]. Besides, they efficiently

manipulate the response of their host cells using simple molecular cues that trigger programmed cellular behaviors. Interestingly, some of the cell entry mechanisms used by these natural systems can also circumvent the receptor-mediated `canonical´ endo-lysosomal entry route to prevent their degradation or exocytosis.

In the search for new receptor-mediated cell entry routes bypassing the canonical endo-lysosomal vesicular pathway, we decided to investigate the Shiga toxin (ShTx) as a protein-ligand [7]. This toxin, produced by *Shigella dysenteriae* and certain strains of *Escherichia coli*, is a protein that specifically recognizes globotriaosylceramide (GB3 or CD77) [8]. The mechanism of ShTx cell recognition and invasion is one of the most well-known systems of prokaryotic hijacking of eukaryotic response [9]. The toxin penetrates the cytoplasm of the target cells bypassing the endolysosomal pathway, thus avoiding exposure to enzymatic and acid lysosomal media that would destroy the toxin and, in our case, the therapeutic agents [10]. Interestingly, several studies have localized the ShTx receptor in cancer cells of different origins [8, 11–15]. This glycosphingolipid, enriched in membrane microdomains known as lipid rafts, is overexpressed in many multidrug-resistant human tumor cells and is therefore a very interesting receptor for the treatment of malignant neoplasms.

Among all localized and accessible cancers, we have focused on the squamous cell carcinoma head and neck (HNC). This includes a great heterogeneity of tumors that arise from the mucosal surfaces of the oral cavity, that are difficult to treat, and are typically characterized by recurrences that are often fatal. Indeed, this is the sixth most common form of cancer [16, 17], with survival rates of approximately 40–50% five years after diagnosis [18, 19]. This cancer is generally removed surgically and then treated with adjuvant radiotherapy or chemoradiotherapy [16]. However, fatal recurrences are very common due to poor detection of preneoplastic areas, deficient removal of the affected tissue, and poor penetration of the systemic drug into the tumoral mass.

We believe HNC is a clear example of a heterogeneous localized malignancy that could significantly benefit from the local (topical) treatment with targeted nanomedicines for both, diagnosis and treatment. Interestingly, previous studies have established that GB3 is a marker for preneoplastic and malignant HNC cells [13]. Thus, given that this type of cancer is accessible, our hypothesis is to use nanoparticles targeted by ShTxB as a local treatment to avoid possible systemic toxicity. In this study, we genetically engineered an innocuous ShTx-based ligand protein for conjugation with gold nanorods (AuNRs) to identify and kill preneoplastic and malignant HNC cells by local photohyperthermia.

Results And Discussion

Targeting ligand design

The ShTx belongs to the AB5 toxin family secreted by some pathogenic bacteria (Figure 1a) *[20]. All these toxins share a similar structure and follow identical mechanisms for entering the targeted cells. From the structural point of view, ShTx is composed of 6 (1+5) polypeptides (Figure 1a). The "A" subunit is the catalytic subunit that, upon internalization, interferes with the regular functions of the host cell. The rest*

*of the toxin comprises five identical copies of the "B" subunit, which assemble into a homo*pentamer surrounding *the "A" subunit. Each "B" subunit can contact the receptor on the target cell membrane by triggering clustering u*pon coupling, thereby provoking membrane ruffling *[7,20–23].* \

The ShTx "B" subunits are innocuous high-affinity GB3 natural ligands [7,24] that have been used to successfully drive fluorophores,[25,26] radionuclides [27], drugs [11,28], or even nanoparticles [12] to the cytoplasm of GB3 positive (GB3+ve) cells. In the view of these results, we proposed to use this fragment of the ShTx protein as a ligand to target multifunctional photoactivatable nanomaterials to GB3 positive (GB3+ve) squamous carcinoma cells. To do this, we genetically engineered a customized protein fusing the *ShTx "B"* subunit to a cationic peptide to allow the electrostatic functionalization of nanomaterials following a bioconjugation method previously described (Experimental Section) [12,29]. In brief, the designed chimera protein named ShTxB:6xHis (hereafter ShTxB) containing the ShTx *"B" subunit* (UniProtKB ref. P09386) was genetically linked to its C-terminus to a *hexahistidine tag (*6xHis) (Figure S1). This cationic peptide creates an electrostatic zipper with the negative surface of the particle that positions the ligand-domain of the protein correctly oriented on the nanoparticle surface (Figure 1a)[29]. This functionalization method also reduces the non-specific protein biofouling and it is very stable upon exposure to physiological conditions (> 72 h) [29].

AuNRs synthesis and functionalization

To destroy the cancer cells topically we designed nanomaterials capable of producing hyperthermia upon laser illumination. Among the wide variety of available plasmonic nanomaterials, AuNRs are arguably the most commonly used system [30], on account of their reproducible and versatile synthesis methods, and tunable localized surface plasmon resonances (LSPR) [31]. For the present study, we synthesized AuNRs with dimensions of *ca.* 55 nm x 13 nm (Figures 1b, S2), resulting in a longitudinal LSPR band centered at 803 nm, resonant with an 808 nm laser diode, within the first biological window. Details of the synthesis protocol can be found elsewhere [30]. For *in cellulo* localization purposes, AuNRs were coated with a *ca.* 35 nm thick Rhodamine B isothiocyanate (RBITC) stained amorphous silica shell (AuNRs@SiO_2), prepared following the procedure described previously [32]. Before activation, the resulting AuNRs@SiO_2:RBTIC particles displayed no detectable toxicity at 5-15 µg/mL dosages when applied to human pharynx epithelial carcinoma after 96 h (Figure S3).

The design was finalized by biofunctionalization of the AuNRs@SiO_2:RBTIC with an ShTxB ligand-protein layer (Figure 1c). Bioconjugation of the nanoparticles was done by incubation in a 0.5 mg/mL solution of ShTxB:6xHis protein produced in bacteria and subsequently purified following standard procedures (see details in the Supporting Information). The presence of ShTxB on the AuNRs@SiO_2:RBTIC surface was biochemically validated by SDS-PAGE analysis (Figure 1d, S1b).

Affinity of functionalized nanomaterials for HNC cells

To determine the affinity of the functionalized AuNRs@SiO_2:RBTIC@ShTxB for HNC cells bearing the GB3 receptor we chose Detroit 562 cells from human pharynx epithelial carcinoma derived from a metastatic pleural effusion. As negative controls, we used MCF-7 human breast cancer cells lacking the GB3 receptor (GB3-ve) (Supporting Information). Confirmation of the presence/absence of the receptor in both cell models was investigated by immunostaining with anti-GB3 antibodies using two technologies, flow cytometry and confocal microscopy (Figure S4). Upon validation of the models, we tested the affinity of the nanoconjugates for the neoplastic cells. To do this, 2D cultures of the two cell types were exposed in parallel to 5 µg/mL of nanoparticles functionalized with ShTxB in culture media for 2 h. At this time, the cells were fixed and processed for flow cytometry for quantification of the captured functionalized nanorods (Figure 2a). We found that, compared to controls (<2% cells containing nanorods), more than 90% of HNC GB3+ve cells (Detroit 562) captured nanoparticles during this incubation period. This finding was next validated using confocal microscopy. Figure 2b shows how, 2h after nanoparticle incubation with the cells, the grouped nanorods co-localized with the cytoplasmic membrane presumably coupled with clustered GB3 receptors (orange arrows). This finding was also supported by TEM images of ultrathin sections of the cells (Figures 2c, 2d). Together, these results support the hypothesis that ShTxB-coated nanorods efficiently interact with GB3 receptors on HNC cells penetrating the cellular cytoplasm of these neoplastic cells

Photohyperthermia to destroy HNC with the ShTxB functionalized AuNRs

The morphology of the AuNRs was designed to induce heating by illumination with an LD of 808 nm, coinciding with the first biological window. For these studies, HNC cells were exposed to AuNR@SiO_2@ShTxB for 2 h, were washed, and then collected into pellets of approximately 2-mm roughly resembling solid microtumors, (see the experimental design in Figure 3a). These were irradiated for 3 or 10 min with an unfocused 1 W fiber LD at 808 nm, in resonance with the longitudinal LSPR of AuNRs. After irradiation, cells were immediately reseeded and allowed to grow for 24 h before live/dead quantification by flow cytometry (Figure 3a).

The study revealed that a 3-minute laser exposure was sufficient to kill ca. 50% of GB3+ve neoplastic cells that contained AuNR@SiO_2@ShTxB (Figure 3b). Longer irradiation periods (10 min) eliminated *ca.* 80% of the HNC cells (Figure 3c). In contrast, control GB3-ve cells treated in parallel were almost unaffected by exposure to nanomaterials and laser radiation. (Figure 3b).

As a complement, we also investigated this effect in 2D cultures of HNC neoplastic cells. Following the experimental depicted in Figure 4a, we incubated cultures of Detroit 562 cells with AuNRs@SiO_2@ShTxB (5 µg/mL for 3 h) and exposed the cultures to an 808 nm unfocused laser irradiation for 10 min. Figure 4b shows how, approximately 1 h after irradiation, dead cells (stained in red) appear in the treated area (yellow circle). Dead cells progressively detach from the culture substrate, leaving a clearly visible cell-free area 24 h after irradiation. The delay in the onset of cell death suggested the activation of death cascade processes triggered from the inside out, suggesting apoptosis (see Figure 3b). This process of cell death is more desirable than the necrosis that is normally triggered when cells are abruptly destroyed with heat

using external sources or when heated nanoparticles pierce the cytoplasmic membrane. As expected, no cell death was detected in control cultures irradiated without nanoparticles, or cultures treated with nanoparticles but not laser (Figure S5a). In the experiment, the temperature in the culture medium was measured during irradiation and no significant changes were observed (Figure S5b). In summary, these results demonstrate that AuNRs functionalized with the ligand-protein ShTxB produce a potent and highly selective cytotoxic effect on HNC cells after laser treatment.

The photothermal effect of functionalized AuNRs *in vivo*

To assess whether this treatment could be transferred to the clinic, we moved on to preclinical models of study. To do this, we reproduced a well-established squamous cell carcinoma murine model that has been validated in many previous HNC studies using the carcinogen 4-NQO (Supporting Information) [33–35]. Treatment of mice with this substance in the drinking water generates visible squamous cell carcinoma lesions on the surfaces of the tongues of the treated mice. Once the tumors were visible, mice were treated with AuNRs@SiO2:RBTIC@ShTxB resuspended in drinking water for 24 h. (please see the experimental design in Figure 5a).

After sacrifice, the surfaces of the tongues of the treated mice, visibly affected by verrucous and pseudo-hyperplastic carcinomas, were locally irradiated once with a 1 W unfocused LD fiber at 808 nm for 10 min. The macroscopic changes are indicated with empty blue arrows (Figure 5b, top). The changes resulting from this single treatment are most clearly seen at the microscopic level in tissue sections. Among others, differences in keratosis before (solid white arrow) and after (black arrows) treatment are evident. Histologically, LD irradiation at 808 nm produced conspicuous destruction on the surface of the warty lesions accompanied by a reduction in the thickness of the GB3+ve cell layer (Figure 5b, empty white arrows). Furthermore, similar to what was observed in 2D cultures treated with nanoparticles and irradiated, the superficial epithelium of the irradiated area was partially detached from the underlying tissues, thus supporting a localized photo-induced hyperthermic effect. These findings suggest that this treatment was effective on the superficial tissue layer and that it could be performed repeatedly on the affected area, hence destroying the affected GB3+ve neoplastic tissue layer by layer until achieving the total elimination of tumor and precancerous cells. Alternatively, the treatment could also be applied after surgical removal of the entire tumor to ensure that there are no precancerous areas in the vicinity that could lead to new relapses.

Efficacy of AuNR@SiO2:RBTIC@ShTxB treatment in biopsy samples from patients diagnosed with HNC

Finally, we explore the effect of AuNRs@SiO2@ShTxB and laser treatment on human cell cultures grown from clinical specimen biopsies of HNC squamous cell carcinomas located on the floor of the mouth (MASCC, moderately aggressive, intermediate grade), and retromolar trigone (ASCC, high grade, aggressive) (please see Supporting Information). Control cells were isolated from a healthy human biopsy sample from the cheek inner mucosa.

As a preliminary test we first verified if cells grown from the cancer biopsies were GB3+ve and, secondly, if, as in the cell lines used previously, these cells captured the functionalized nanoparticles. Figure 6 shows how, compared to control cells obtained from healthy individuals, cells from the HNC patients displayed abundant GB3 on their surfaces (yellow channel). And, as previously observed for cell ines, we also found that the HNC biopsy cells internalized a significant amount of AuNRs@SiO2:RBTIC@ShTxB nanoparticles (red channel) into their cytoplasm compared to healthy mucosal cells.

After these preliminary tests, we applied a procedure similar to that described in Figure 4 to these biopsy cell cultures (Figure 7a). For this study, cultures of patients' cells were exposed to 5 µg/mL of AuNRs@SiO_2@ShTxB for 2 h. Thereafter, cultures were irradiated for 10 min with the LD 808 nm and grown for 24 h before analysis. As seen for cell lines, Figure 7b shows the efficient removal of cancer cells in the culture irradiation area. This treatment, which was highly effective on the cells of the carcinoma sample (MASCC and ASCC), did not affect healthy cells of the oral mucosa treated identically in parallel. No detectable cell death occurred in controls irradiated with the LD but no particles (Figure S6).

In summary, this study demonstrates that the local (topical) application of nanomaterials targeted by high-affinity natural ligands in combination with photo-hyperthermia has enormous potential as a treatment for localized neoplasms such as HNC, the seventh most common cancer worldwide. The current treatment of choice for this type of tumor is surgery followed by chemotherapy or immunotherapy. Unfortunately, the high mortality of these patients (*ca.* 50% in the 5 years after diagnosis) is due to poor penetration of chemotherapy into the tumor. So the treatment requires the use of very high doses of cytotoxic chemotherapy or radical surgeries that significantly worsen the quality of life of patients. Immunotherapy on the other hand usually gives spectacular but very transitory results due to tumor resistance.

Here we propose using ShTxB functionalized nanotherapies to selectively target and destroy the neoplastic cells. This may be used as an adjuvant method to enhance the effects of these standard treatments, improving the recovery and survival rates of patients.

Conclusion

We propose the use of targeted topical nanobiotechnology in support of existing diagnostic and therapeutic tools to prevent recurrences. As shown in our *in vivo* model, the treatment would consist of applying the functionalized nanoparticles locally, i.e. by direct deposit or mouthwash. The ShTxB-coated nanoparticles would specifically bind to receptors on preneoplastic and malignant cells, penetrating their interior, and ultimately destroying the cancer cells upon activation by near-infrared LD light irradiation locally.

There are many advantages related to the topical use of these nanoparticles. Among others, they do not cause an immunoreaction, nor are prematurely eliminated by phagocytes since they are not supplied parenterally. In addition, we have shown that these nanosystems are safe by design until laser irradiation so, in case of being swallowed they can travel along the digestive tract until they are safely eliminated. The nanoparticles presented herein could also be used for the treatment of cancers in other regions of the digestive tract where GB3 has also been reported, including cancers of the esophagus, stomach, or colon *[8,11].* In these cases, a laser fiber could be coupled to an endoscope system to guarantee access to the relevant areas of the digestive tract. In addition, there is the possibility of using the ShTxB toxin fragment as a biosensor to detect these neoplasms that, in their early stages, often escape detection by standard clinical methods. For this, a double wavelength laser could be used. Green laser light would be used to identify the area affected by the tumor (GB3+ve) delimited by the red fluorescence of the fluorescent AuNRs and, switching to a NIR LD wavelength of 808 nm, photohyperthermia treatment to kill the neoplastic cells directly or repeatedly, layer by layer over the affected area.

Methods

Nanorods synthesis, SiO_2 coating, and characterization.

Gold nanorods (AuNRs) in CTAB (Cetyltrimethylammonium Bromide) were synthesized using salicylic acid as an additive as previously described [36,37]. For coating AuNRs with silica, CTAB on the surface was exchanged with mPEG-SH. Excess CTAB was washed by repeated centrifugation, AuNRs were resuspended in Milli-Q water and a solution of mPEG-SH (50 molecules/nm^2) was added dropwise. After 1 h of stirring AuNRs were washed and finally redispersed in ethanol. Silica coating was performed by mixing AuNRs ([Au] = 0.5 mM) with the appropriate amount of H_2O (10.55 M), NH_3 (0.2M), and tetraethyl orthosilicate (TEOS) solution (1 mM) and allowing reaction for 6 h at RT [38]. The fluorophore Rhodamine B isothiocyanate (RBITC) was conjugated to APMS and added in subsequent shell re-growth steps allowing its conjugation to SiO_2 [32]. Fluorescently coated AuNRs were washed by repeated cycles of centrifugation/redispersion in ethanol. All reagents were obtained from Sigma-Aldrich, except ethanol (96%) that was purchased from Scharlab. Ethanol-dispersed nanorods were adsorbed onto a Lacey copper grid (400 mesh, EM Resolutions) and characterized using a JEM 1011 (JEOL) transmission electron microscope (Figure S1).

Gene synthesis, protein expression, and purification.

ShTxB:6xHis recombinant gene construct was synthesized by General Biosystems, Inc. (Morrisville, USA) and was cloned in pET-15b plasmid systems (Novagen, Merck KGaA, Spain). One Shot™ BL21(DE3) E. coli (NZYTech, Portugal) cells were transformed with the expression vector. Bacterial cultures were grown in Luria-Bertani (LB) broth supplemented with 100 µg/mL ampicillin and 35 µg/mL chloramphenicol until A600 ca. 0.6. The expression of the protein was induced by adding 0.1 mM isopropyl b-D thiogalactopyranoside (IPTG). Cells were collected after 4 hours by centrifugation and were resuspended

in 50 mM NaPi, 300 mM NaCl, pH 8.0 with 1 mg/mL lysozyme, and protease inhibitors (Pierce, Thermo Fischer, Spain).

Bacterial cell lysates were obtained by probe sonication (5 ´ 15 s pulses at 130 W, 65% amplitude, with 15 s intervals, at 4 °C), and insoluble material was removed by centrifugation. Bacterial soluble protein lysate was loaded onto pre-equilibrated Ni-TED columns (Protino® Ni-TED, Macherey-Nagel GmbH & Co., Düren, Germany). The recombinant His-tagged protein was eluted in buffer supplemented with 250 mM imidazole. Finally, PD-10 desalting Columns (GE Healthcare, Chicago, USA) were used to remove the imidazole and to exchange buffer for PBS.

Protein bioconjugation on particles, SDS-PAGE protein analysis.

Nanorods were functionalized with 0.5 mg/mL of the protein solution (saturating amounts) in PBS during 3 ´ 2 s mild sonication at room temperature. For SDS-PAGE, the protein functionalized on the particles was stripped using Laemmli sample buffer 1´ (BioRad) at 90 ºC for 2 min. SDS-PAGE electrophoresis was performed using Mini-Protean® precast gels (BioRad). Protein analysis was performed on Coomassie blue-stained gels that were scanned using the BioRad GelDoc EZ system.

Cell culture and compacted pellet (micro tumor) conditions.

Detroit 562 cells, human pharynx epithelial carcinoma cells derived from a metastatic pleural effusion, and MCF-7, human breast cancer cells, were obtained from ATCC (Ref. CCL-138 and HTB-22 respectively). Detroit 562 cells were grown in Modified Eagle´s Medium and MCF-7 cells in Dulbecco´s Modified Eagle´s Medium (Sigma) containing 10% bovine serum. Both cell lines were kept in standard conditions. MCF7 cells were used as controls (GB3-ve) after characterization with the anti-GB3 antibody (Figure S4). A total of 500.000 cells were washed, trypsinized, and centrifuged at 1000 rpm for 5 minutes. The supernatant was removed, and pellets were re-suspended in 50 µL of culture media to create a cell pellet that was used as a microtumor.

Staining, fluorescent, and electron microscopy imaging.

Cells were exposed to 5 µg/mL of bioconjugated AuNRs@SiO_2:RBTIC@ShTxB particles for 3 hours. Cells were fixed with 4% paraformaldehyde, were stained with Hoechst 33258 (Sigma-Aldrich®), Acridine Orange (Sigma-Aldrich®) for live cells, or ethidium bromide (Sigma) for dead cells. Alexa 647-anti-Human CD77 (BD Pharmingen™, UK) was used for immunostaining the GB3 receptor. Confocal images were taken with a Nikon A1R microscope. All fluorescent images are pseudo-colored. Cell samples processed for electron microscopy were fixed with 3% glutaraldehyde in 0.12 M PBS for 24 hours and were post-fixed in 2% buffered osmium tetroxide, dehydrated in a graded acetone series, and embedded in Araldite. Ultrathin sections of *ca.* 70 nm thick, were obtained on an LKB ultramicrotome, stained with lead citrate and uranyl acetate. TEM was performed using a JEOL JEM 1011 operated at 100 kV.

Flow cytometry.

Cell death experiments were performed using 10^6 Detroit and MCF-7 cells. Following manufacturer instructions, these cells were stained with Annexin V-FITC kit (Immunostep) for 15 min. and then passed through the cytometer (CytoFLEX, Beckman Coulter). Quantitative GB3 expression was validated and measured in a total of 10.000 Detroit and MCF-7 cells immunostained with Alexa 647-anti-Human CD77 (BD Pharmingen™, UK) for 30 minutes and then fixed in 4% paraformaldehyde (Figure S4). Qualitative interaction of AuNRs@SiO_2@ShTxB in cells was performed using 10.000 Detroit 562 and MCF-7 cells. Cells were exposed to the nanoparticles for 3h, washed, and passed through the cytometer. Data were analyzed using the CytExpert software.

Murine model and tissue processing.

In vivo experiments were designed and performed to minimize the use of animals. Ethical permissions for this study were requested, approved, and obtained from the Bioethics Committee University of Cantabria, General Directorate of Livestock, Government of Cantabria (Project Ref PI-11-21). C57BL/6 mice (12 weeks old) were housed with a 12 h light/dark cycle with free provision of food and water at the Experimentation Service of the University of Cantabria. The animals were maintained, handled, and sacrificed following the directive 2010/63/UE. The preclinical model of oral carcinogenesis was produced using the carcinogen 4-Nitro-quinoline-1-oxide (4-NQO, Sigma Aldrich) as previously described [33–35]. In brief, C57BL/6 mice were drinking water with 100 µg/mL of 4-NQO for 16 weeks (water was changed once a week). After 16 weeks of carcinogen treatment, the mice with visible lesions in the oral cavity were treated with 5 µg/mL of AuNRs@SiO_2@ShTxB in the drinking water (approximately 1 mg/Kg mice total) for 24 hours before sacrifice. For the laser irradiation, mice were humanely sacrificed and the tissues were dissected and immediately irradiated as indicated in the text. The irradiation procedure was performed only once. The tissues were fixed in 10% formalin, embedded in paraffin, sectioned (4 µm thick), deparaffinized, stained with hematoxylin-eosin, or preserved in optimal cutting temperature compound (OCT) at -80 ^oC to be cryosectioned. Approximately 6 µm cryostat sections were fixed in paraformaldehyde 4%, immunostained with Alexa 647-anti-Human CD77 (BD Pharmingen™, UK), and with Hoechst.

Human biopsies and cell culture of head and neck squamous carcinomas.

Ethical permissions for this study were requested, approved, and obtained from the Ethical Committee for Clinical Research of Cantabria Council, Spain (Ref. 2017.259). In all cases, human tissue material discarded after surgery was obtained with written consent presented by clinicians to the patient and was treated anonymously. Biopsy sample cell cultures were grown from biopsies of malignancies localized at the floor of the mouth (MASCC, moderately aggressive, intermediate grade), and retromolar trigone (ASCC, high grade, aggressive). The grade of aggressiveness was characterized by the clinician. Control cells were isolated from a healthy human biopsy (cheek inner mucosa). Biopsies were cut into pieces and washed twice with PBS-EDTA, 100 U/mL penicillin-streptomycin (Pen/Strep), and 0.5 µg/mL Amphotericin B. Pieces were then washed twice with 1x PBS, 100 U/mL Pen/Strep, and 0.5 µg/mL Amphotericin B and incubated with agitation at 37 °C for 4 rounds of 15 min with 0.075% trypsin, 2.5

mg/mL collagenase P, 1´ PBS, 100U/mL Pen/Strep and 0.5 µg/mL Amphotericin B. Isolated keratinocytes were co-cultured with a feeder layer of (3T3)-J2 mouse fibroblast feeder layer (previously inactivated with mitomycin C).

HNSCC and healthy primary keratinocytes were cultured in modified Rheinwald FAD medium [39,40]: 3:1 v/v Dulbecco's Modified Eagle Medium – Ham's F12, 5% fetal bovine serum, 0.5 µg/mL hydrocortisone, 5 ng/mL epidermal growth factor, 9 ng/mL cholera toxin, $1.8´10^{-4}$ M adenine, 5 µg/mL insulin, 2 mM L-glutamine, 0.75 mM sodium pyruvate, and 100 U/mL Pen/Strep. Mouse fibroblast 3T3-J2 cell line used as feeder layer was cultured in Dulbecco medium with 10% donor calf serum and 100 U/mL Pen/Strep.

Laser microtumor irradiation.

Detroit 562 and control MCF-7 cells were exposed to 5 µg/mL and 10 µg/mL of AuNRs@SiO_2@ShTxB for 3h. Then cells were washed, pelleted into microtumors, and irradiated with an unfocused NIR laser (808 nm LD, 1 W) for 10 min. After irradiation cells were placed back in culture plates in the incubator for another 24 hours. After this period, cells were stained with a dead cell apoptosis kit with AnnexinV-FITC and PI, for flow cytometric analysis and confocal microscopy at 0 and 24h.

2D/3D culture irradiation.

Cultures of neoplastic or normal cells from oral biopsies cells were treated with 5 µg/mL AuNRs@SiO_2@ShTxB for 3 h. After removal of the particles in the media, cultures were irradiated with the 808 nm LD for 10 min directly on the plate. *In vivo* tumor irradiation: Once verrucous cancerous lesions were visible in the oral cavity, the mice were supplied with water containing 10 µg/mL of the AuNRs@SiO_2:RBTIC@ShTxB particles for 12h. The mice were euthanized, and the tongues were dissected and photographed. Then, tongues were irradiated with an 808 laser for 5 min. Tissue sections after irradiation were processed and analyzed as previously described.

Statistical analysis.

Student's *t*-test analysis was used for statistical analysis. In Figure 3, significance that was established for a (*) $p < 0.025$ or a (**) $p < 0.005$. Quantitative results are expressed as mean values with their corresponding standard error bars. These statistical analyses were done using SPSS, version 19.0.

Declarations

Acknowledgments

We are grateful to Débora Muñoz for her technical support.

Authors' contribution

ENP and LGH contributed equally to this work. MLF wrote the main manuscript text and ENP and LGH prepared figures. JVG, AG, and FGR obtained and cultured the human biopsies. RV, ASI, and LLM designed and prepared the nanomaterials. ENP and MLF designed, prepared the protein, and functionalized the NR. LGH performed the in vivo and biopsy experiments. All authors reviewed the manuscript. All authors read and approved the final manuscript.

Funding

The authors are grateful for the financial support. MLF acknowledges ISCIII Grants PI19/00349 and DTS19/00033, co-funded by the European Regional Development Fund, "Investing in your future"; COST action Nano2Clinic CA17140, and IDIVAL for the PREVAL16/02, INNVAL18/28, INNVAL20/13 and INNVAL21/19 projects. L.M.L.-M. acknowledges funding from the European Research Council (ERC AdG 787510, 4DbioSERS) and the María de Maeztu Units of Excellence Program from the Spanish State Research Agency (Grant No. MDM-2017-0720). RV acknowledges financial support from Spanish Ministerio de Ciencia, Innovación y Universidades (PGC2018-101464-B-I00) and HIPERNANO RED2018-102626-T). AG acknowledges ISCIII/FIS-FEDER Grant PI20/00880. JG acknowledges the predoctoral scholarship from Asociación Española Contra el Cáncer (AECC; Spain), PRDCA19003GALA. Graphs in Figures 1c, 2a, 3a, and 4a have been created with BioRender.com.

Availability of data and materials

The datasets used and/or analyzed during the current study are available from the corresponding author on reasonable request.

Ethics approval and consent to participate

All experimental procedures involving animals performed in this study were previously approved and certified (Ref. PI-11-21) by the Bioethics Committee University of Cantabria, General Directorate of Livestock, Government of Cantabria, and the Ethical Committee for Clinical Research of Cantabria Council (Ref. 2017.259).

Consent for publication

Not applicable.

Competing interests

The authors declare that they have no competing interests.

References

1. Walkey CD, Chan WCW. Understanding and controlling the interaction of nanomaterials with proteins in a physiological environment. Chem Soc Rev. 2012;41:2780–99.

2. Nel AE, Mädler L, Velegol D, Xia T, Hoek EM V., Somasundaran P, et al. Understanding biophysicochemical interactions at the nano-bio interface. Nat Mater. Nature Publishing Group; 2009;8:543–57.
3. Monopoli MP, Åberg C, Salvati A, Dawson KA. Biomolecular coronas provide the biological identity of nanosized materials. Nat Nanotechnol. Nature Research; 2012;7:779–86.
4. Wilhelm S, Tavares AJ, Dai Q, Ohta S, Audet J, Dvorak HF, et al. Analysis of nanoparticle delivery to tumours. Nat Rev Mater. Nature Publishing Group; 2016;1:16014.
5. Hasegawa K, Hu C, Nakamura T, Marks JD, Russell SJ, Peng K-W. Affinity Thresholds for Membrane Fusion Triggering by Viral Glycoproteins. J Virol. American Society for Microbiology; 2007;81:13149–57.
6. MacKenzie CR, Hirama T, Lee KK, Altman E, Young NM. Quantitative analysis of bacterial toxin affinity and specificity for glycolipid receptors by surface plasmon resonance. J Biol Chem. American Society for Biochemistry and Molecular Biology; 1997;272:5533–8.
7. Melton-Celsa AR. Shiga Toxin (Stx) Classification, Structure, and Function. Microbiol Spectr. 2014;2 (4):2.
8. Gariépy J. The use of Shiga-like toxin 1 in cancer therapy. Crit Rev Oncol Hematol. 2001;39:99–106.
9. Lingwood C. Therapeutic uses of bacterial subunit toxins. Toxins. 2021;13.
10. Luginbuehl V, Meier N, Kovar K, Rohrer J. Intracellular drug delivery: Potential usefulness of engineered Shiga toxin subunit B for targeted cancer therapy. Biotechnol Adv. 2018;36:613–23.
11. Geyer PE, Maak M, Nitsche U, Perl M, Novotny A, Slotta-Huspenina J, et al. Gastric Adenocarcinomas Express the Glycosphingolipid Gb3/CD77: Targeting of Gastric Cancer Cells with Shiga Toxin B-Subunit. Mol Cancer Ther. American Association for Cancer Research; 2016;15:1008–17.
12. Navarro-Palomares E, García-Hevia L, Padín-González E, Bañobre-López M, Villegas JC, Valiente R, et al. Targeting nanomaterials to head and neck cancer cells using a fragment of the shiga toxin as a potent natural ligand. Cancers. Multidisciplinary Digital Publishing Institute; 2021;13:4920.
13. García-Hevia L, Casafont Í, Morales C, Ovejero V, Lobo D, Fanarraga ML. GB3/CD77 a predictive marker and promising therapeutic target for Head and Neck Cancer. Biomedicines. 2022;10:732.
14. Behnam-Motlagh P, Tyler A, Grankvist K, Johansson A. Verotoxin-1 Treatment or Manipulation of its Receptor Globotriaosylceramide (Gb3) for Reversal of Multidrug Resistance to Cancer Chemotherapy. Toxins 2010, Vol 2, Pages 2467-2477. Molecular Diversity Preservation International; 2010;2:2467–77.
15. Arab S, Russel E, Chapman W, Rosen B, Lingwood C. Expression of the verotoxin receptor glycolipid, globotriaosylceramide, in ovarian hyperplasias. Oncol Res Treat. 1997;9:553–63.
16. Chow L. Head and Neck Cancer. Longo DL, editor. N Engl J Med. 2020;382:60–72.
17. Duprez F, Berwouts D, De Neve W, Bonte K, Boterberg T, Deron P, et al. Distant metastases in head and neck cancer. Head Neck. 2017;39:1733–43.

18. Adkins D, Ley J, Neupane P, Worden F, Sacco AG, Palka K, et al. Palbociclib and cetuximab in platinum-resistant and in cetuximab-resistant human papillomavirus-unrelated head and neck cancer: a multicentre, multigroup, phase 2 trial. Lancet Oncol. 2019;20:1295–305.
19. Leblanc O, Vacher S, Lecerf C, Jeannot E, Klijanienko J, Berger F, et al. Biomarkers of cetuximab resistance in patients with head and neck squamous cell carcinoma. Cancer Biol Med. 2020;17:208–17.
20. Beddoe T, Paton AW, Le Nours J, Rossjohn J, Paton JC. Structure, biological functions and applications of the AB5 toxins. Trends Biochem Sci. 2010;35:411–8.
21. Johannes L, Römer W. Shiga toxins from cell biology to biomedical applications. Nat Rev Microbiol. 2010;8:105–116.
22. Pezeshkian W, Hansen AG, Johannes L, Khandelia H, Shillcock JC, Kumar PBS, et al. Membrane invagination induced by Shiga toxin B-subunit: From molecular structure to tube formation. Soft Matter. 2016;12:5164–71.
23. Römer W, Berland L, Chambon V, Gaus K, Windschiegl B, Tenza D, et al. Shiga toxin induces tubular membrane invaginations for its uptake into cells. Nature. 2007;450:670–5.
24. Ling H, Boodhoo A, Hazes B, Cummings MD, Armstrong GD, Brunton JL, et al. Structure of the Shiga-like toxin I B-pentamer complexed with an analogue of its receptor Gb3. Biochemistry. 1998;37:1777–88.
25. Tavitian B, Viel T, Dransart E, Nemati F, Henry E, Thézé B, et al. In vivo tumor targeting by the B-subunit of shiga toxin. Mol Imaging. 2008;7:239–47.
26. Stimmer L, Dehay S, Nemati F, Massonnet G, Richon S, Decaudin D, et al. Human breast cancer and lymph node metastases express Gb3 and can be targeted by STxB-vectorized chemotherapeutic compounds. BMC Cancer. 2014;14:916.
27. Janssen KP, Vignjevic D, Boisgard R, Falguières T, Bousquet G, Decaudin D, et al. In vivo tumor targeting using a novel intestinal pathogen-based delivery approach. Cancer Res. 2006;66:7230–6.
28. Maak M, Nitsche U, Keller L, Wolf P, Sarr M, Thiebaud M, et al. Tumor-Specific Targeting of Pancreatic Cancer with Shiga Toxin B-Subunit. Mol Cancer Ther. 2011;10:1918–28.
29. Padín-González E, Navarro-Palomares E, Valdivia L, Iturrioz-Rodriguez N, Correa-Duarte MA, Valiente R, et al. A custom-made functionalization method to control the biological identity of nanomaterials. Nanomedicine, Nanotechnology, Biol Med. 2020;102268.
30. Pérez-Juste J, Pastoriza-Santos I, Liz-Marzán LM, Mulvaney P. Gold nanorods: Synthesis, characterization and applications. Coord Chem Rev. 2005;249:1870–901.
31. Scarabelli L, Sánchez-Iglesias A, Pérez-Juste J, Liz-Marzán LM. A “Tips and Tricks” Practical Guide to the Synthesis of Gold Nanorods. J Phys Chem Lett. 2015;6:4270–9.
32. Navarro-Palomares E, González-Saiz P, Renero-Lecuna C, Martín Rodríguez R, Aguado F, González-Alonso D, et al. Dye-doped biodegradable nanoparticle SiO2 coating in zinc- and iron-oxide nanoparticles to improve biocompatibility and in vivo imaging studies. Nanoscale. 2020;12:6164–75.

33. Kanojia D, Vaidya MM. 4-Nitroquinoline-1-oxide induced experimental oral carcinogenesis. Oral Oncol. 2006;42:655–67.
34. Schoop RAL, Noteborn MHM, Baatenburg De Jong RJ. A mouse model for oral squamous cell carcinoma. J Mol Histol. 2009;40:177.
35. Tang XH, Knudsen B, Bemis D, Tickoo S, Gudas LJ. Oral Cavity and Esophageal Carcinogenesis Modeled in Carcinogen-Treated Mice. Clin Cancer Res. 2004;10:301–13.
36. Ding HL, Zhang YX, Wang S, Xu JM, Xu SC, Li GH. Fe3O4@SiO2 core/shell nanoparticles: The silica coating regulations with a single core for different core sizes and shell thicknesses. Chem Mater. 2012;24:4572–80.
37. Scarabelli L, Grzelczak M, Liz-Marzán LM. Tuning gold nanorod synthesis through prereduction with salicylic acid. Chem Mater. 2013;25:4232–8.
38. Fernández-López C, Mateo-Mateo C, Álvarez-Puebla RA, Pérez-Juste J, Pastoriza-Santos I, Liz-Marzán LM. Highly controlled silica coating of PEG-capped metal nanoparticles and preparation of SERS-encoded particles. Langmuir. 2009;25:13894–9.
39. Rheinwald J. Methods for clonal growth and serial cultivation of normal human epidermal keratinocytes and mesothelial cells. Cell growth Div. A Pract. approach.1989.
40. de Pedro I, Galán-Vidal J, Freije A, de Diego E, Gandarillas A. p21CIP1 controls the squamous differentiation response to replication stress. Oncogene. Oncogene; 2021;40:152–62.

Figures

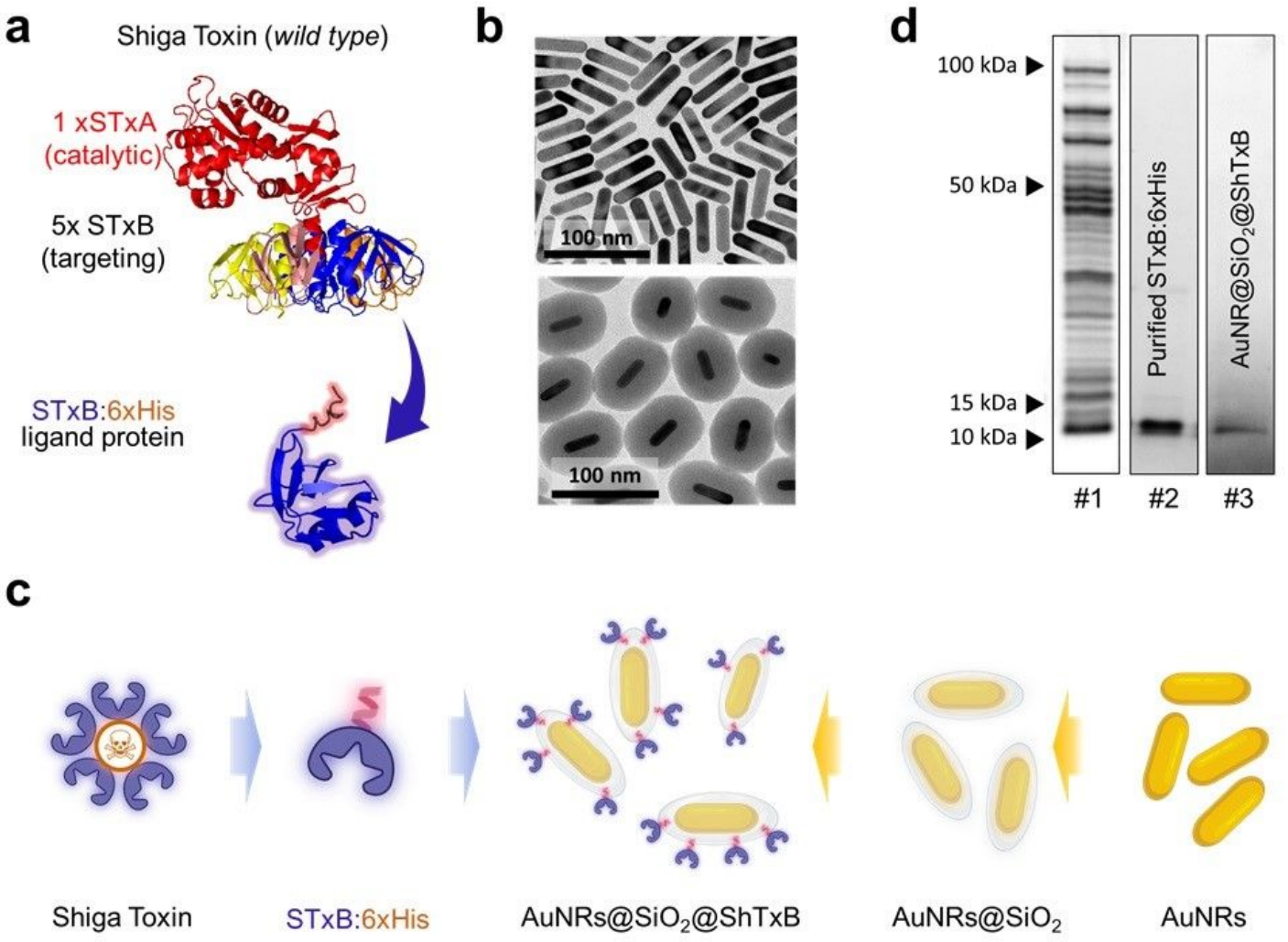

Figure 1

(a) Shiga toxin (ShTx) structure. The predicted structure of the engineered ShTxB-like ligand-protein. A single B domain (ShTxB) (blue) is attached to the 6xHis cationic tail (red). (b) TEM images of AuNRs before and after SiO_2 coating. (c) Diagram of the synthetic steps for production of AuNRs@SiO_2@ShTxB. (d) SDS-PAGE analysis of (#1) Recombinant ShTxB-ligand protein overexpression, (#2) purified ShTxB, and (#3) ShTxB stripped from the functionalized AuNRs@SiO_2@ShTxB.

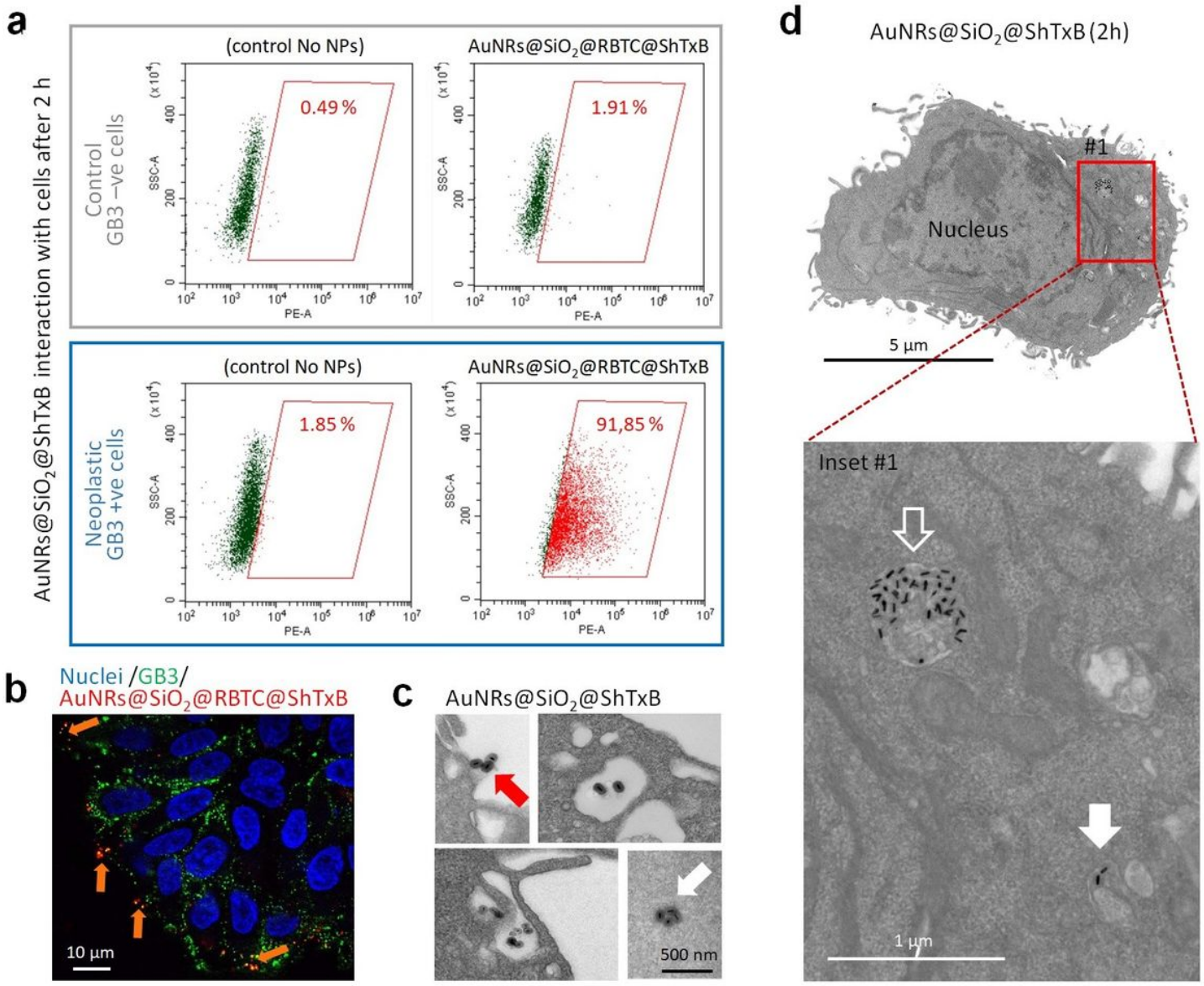

Figure 2

AuNRs@SiO_2:RBTIC@ShTxB cell selectivity. (a) Flow cytometry quantification of the interaction of AuNRs@SiO_2:RBTIC@ShTxB with control (GB3-ve) and HNC (GB3+ve) cells. Cells were exposed to the nanoparticles for 2 h and then washed before fixation and flow cytometry analysis. (b) Confocal microscopy single Z-plane image of human HNC neoplastic cells exposed to 5 µg/mL of the AuNRs@SiO_2:RBTIC@ShTxB (red channel) and live immunostained for GB3 (green channel). Clustered nanorods colocalize with GB3 receptors on the cell surface (orange arrows). (c,d) TEM images of ultrathin sections of HNC neoplastic cells incubated with AuNRs@SiO_2:RBTIC@ShTxB. The NRs contact the cell surface (red arrow). (c) Engulfed particles appear in irregular membranous structures close to the cell edge or the cytosol in the proximity to cytoplasmic membranes. Some NRs can be observed free in the cytosol (white arrow). (d). Image of a whole GB3+ve HNC cell where the functionalised nanoparticles can be found both, in a membranous structure (empty arrow), or free in the cytoplasm (filled arrow).

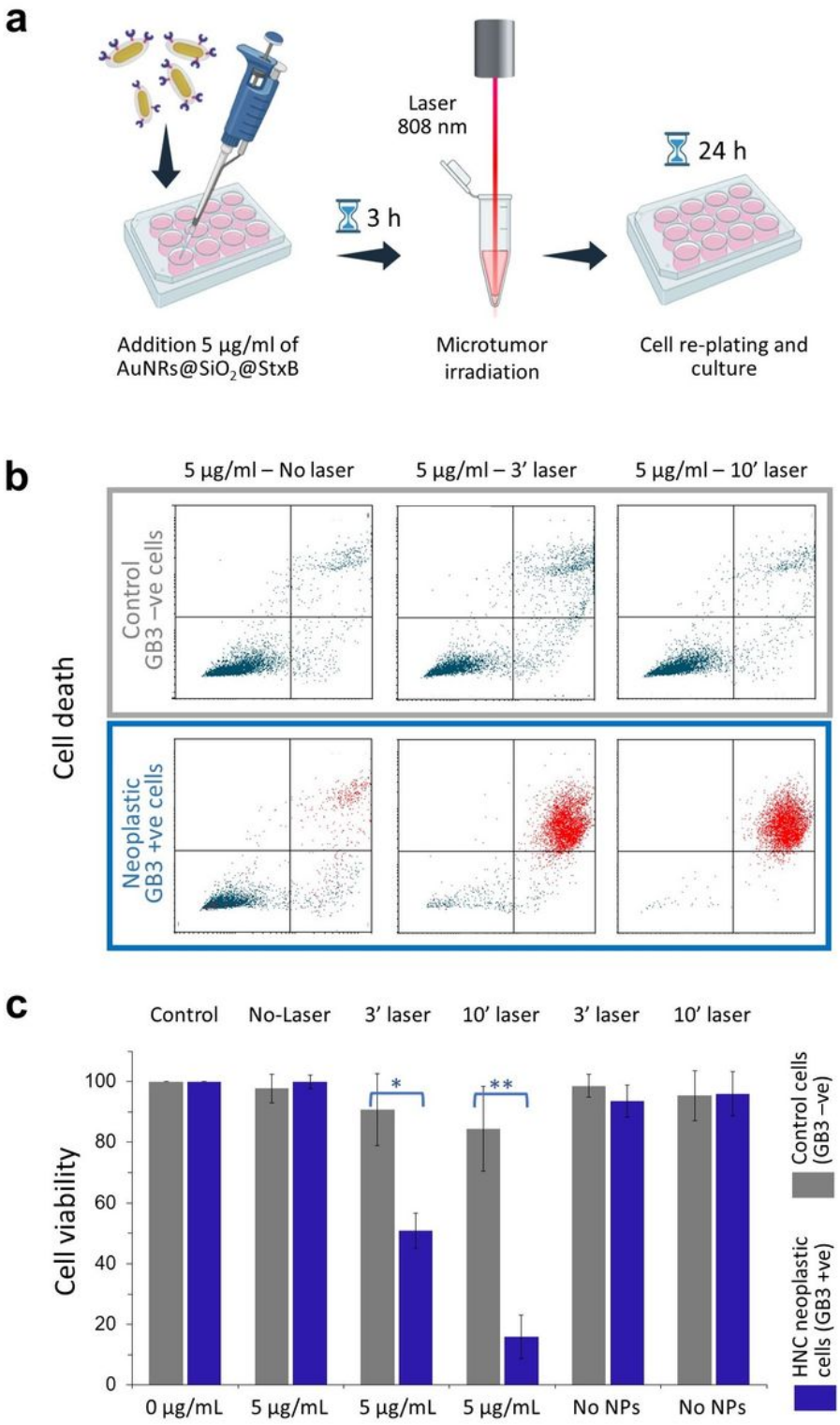

Figure 3

Selective elimination of HNC cancer cells with AuNRs@SiO_2@ShTxB after irradiation. (a) Diagram of the experimental procedure. (b) Live / dead cell quantification 24h after irradiation in control (GB3-ve), and HNC (GB3+ve) cells by AnnexinV-FITC/PI staining and flow cytometry (Figure S4). Dead cells appear in the upper right frame of the chart. (c) Average percentages of cell viability upon LD irradiation to microtumors (approx. 10.000 cells measured per experiment; $n = 3$; * $p < 0.025$; ** $p < 0.005$).

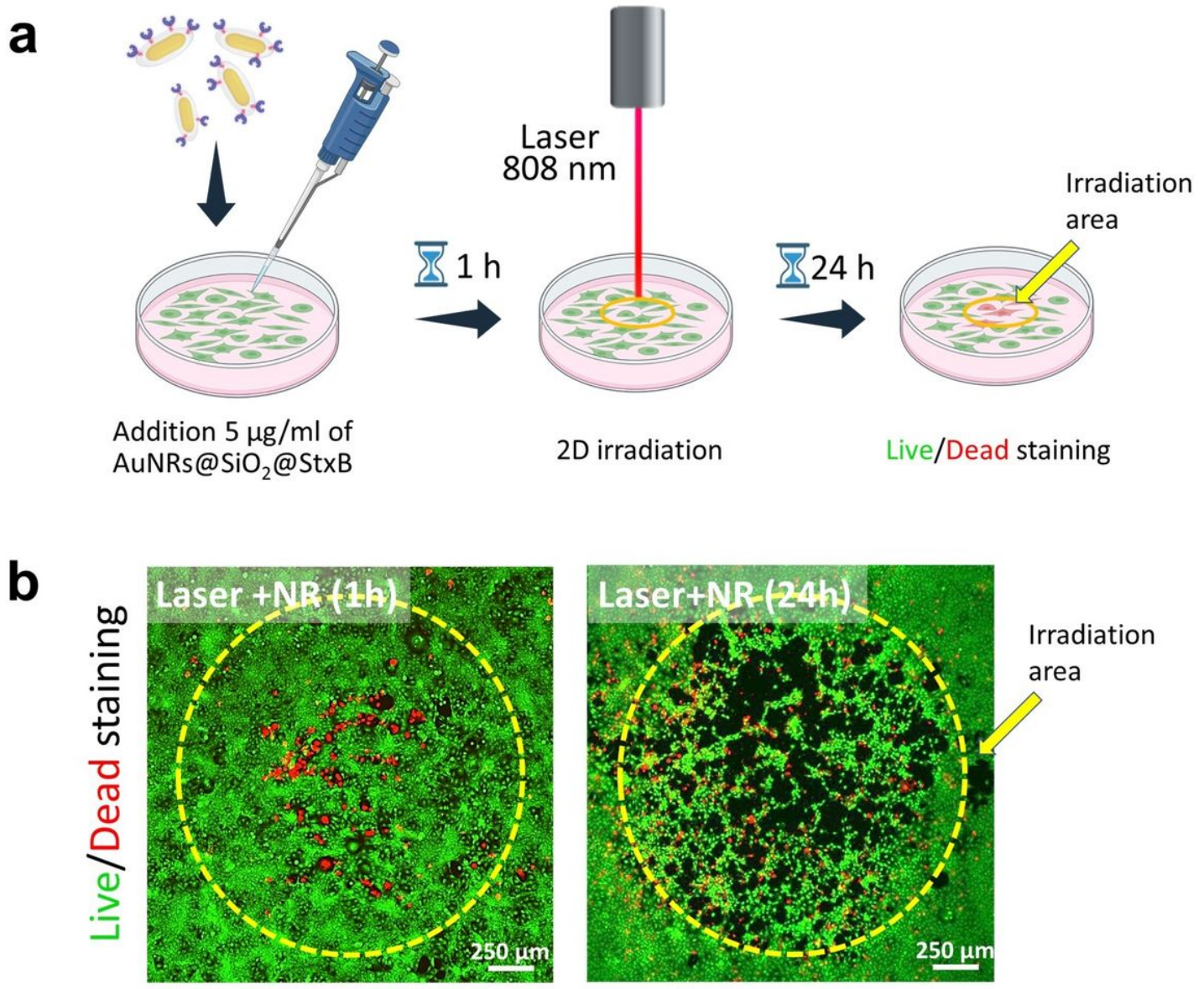

Figure 4

Elimination of cancer cells treated with AuNRs@SiO_2@ShTxB after irradiation in 2D cultures. (a) Diagram of the experimental procedure. (b) Cultures of GB3+ve HNC cells stained with acridine orange (green channel) treated with the AuNRs@SiO_2@ShTxB and exposed to LD irradiation for 10 min (yellow circle). Cells were cultured for the indicated times before live-dead staining. Dead cells (red) are already visible 1 h after irradiation. The detachment of the dead cells from the culture matrix is evident after 24 h.

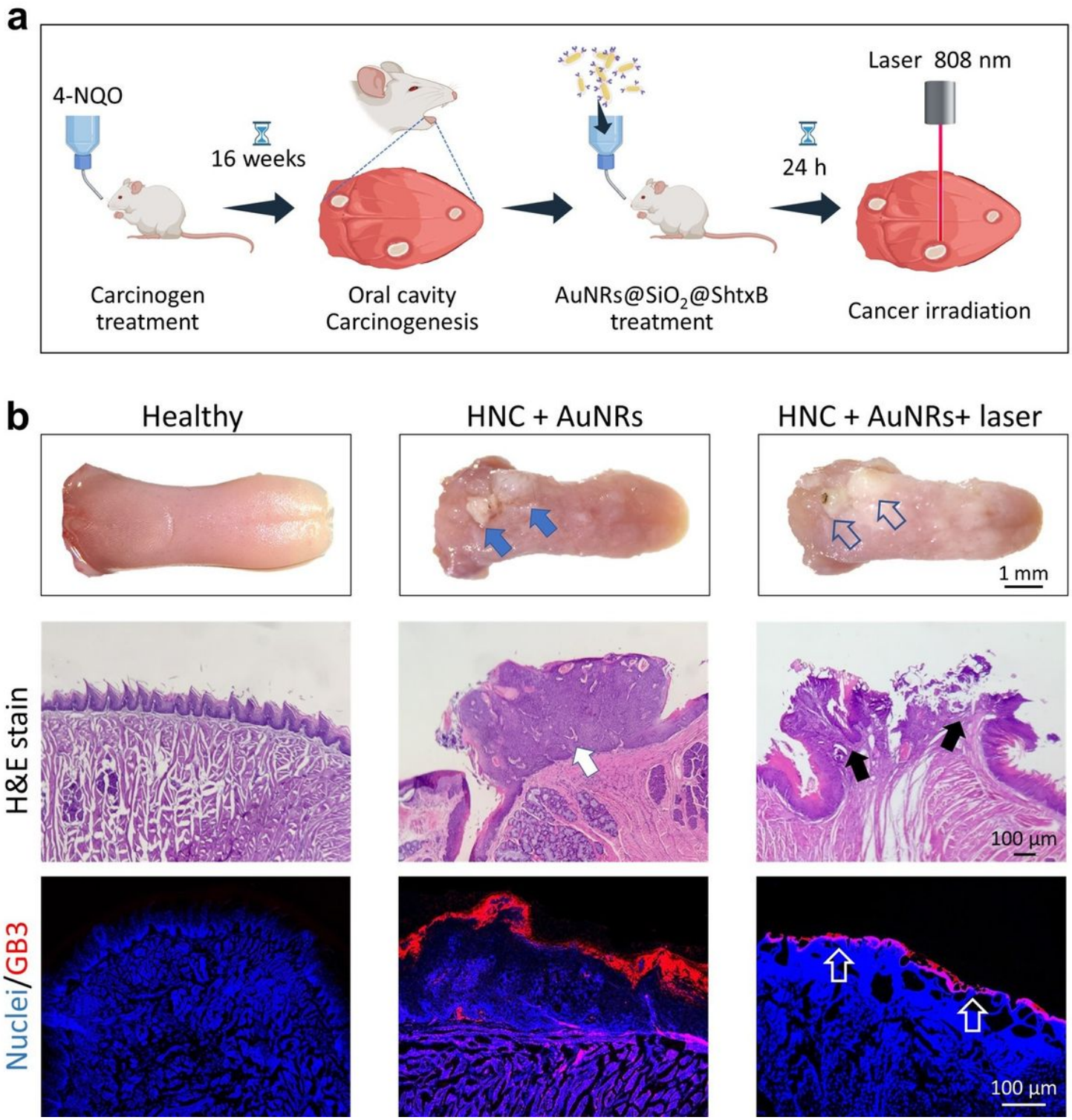

Figure 5

(a) Diagram of murine 4-NQO squamous carcinoma preclinical model and summary of the treatment with AuNRs@SiO_2@ShTxB, followed by photothermal treatment. (b) Post-mortem murine tongues. Blue solid arrows point to representative carcinoma lesions. Empty blue arrows show the same areas after irradiation with an 808 nm LD. These tissues show whiter and swollen lesions. Hematoxylin-eosin-stained sections (H&E) show a patent keratosis at the tongue surface (white arrow) that is visibly affected after

the irradiation treatment (black arrows) (bottom row). Similar sections immunostained with anti-GB3 antibody (red channel). Healthy epithelium does not present a GB3 immunostaining (red channel) whereas tissues from affected animals show a significantly thickened GB3+ve cornified cell layer. The thickness of the GB3+ve layer cells layer is significantly reduced after a single photothermal treatment (empty white arrows).

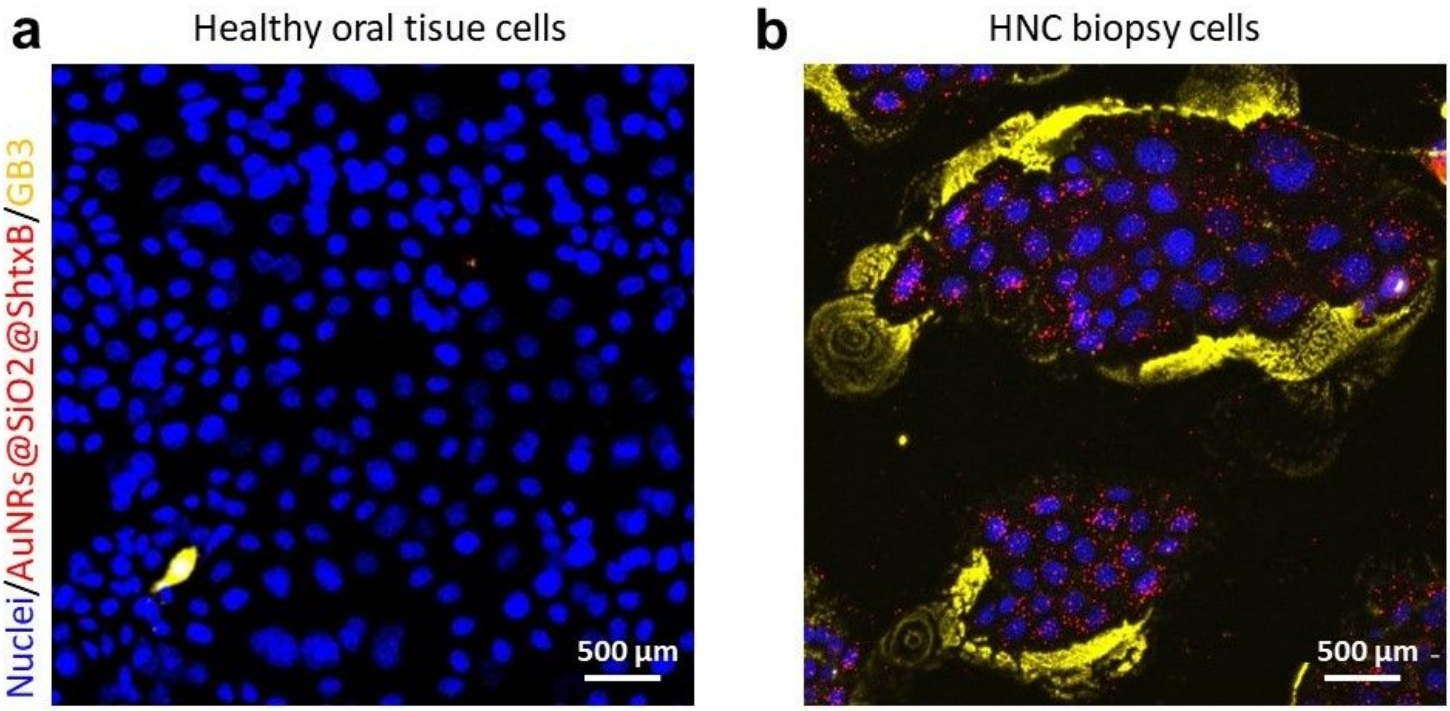

Figure 6

Confocal microscopy projection images of (a) human control cells (healthy oral tissue) and (b) biopsy cells from human aggressive squamous cell carcinoma (ASCC) cells incubated with 5 µg/mL the AuNRs@SiO_2:RBTIC@ShTxB (red channel) live immunostained with anti-GB3 antibody (yellow channel). Intracellular clusters of red nanoparticles can be observed inside HNC patients' cell colonies. Nuclei are stained in blue.

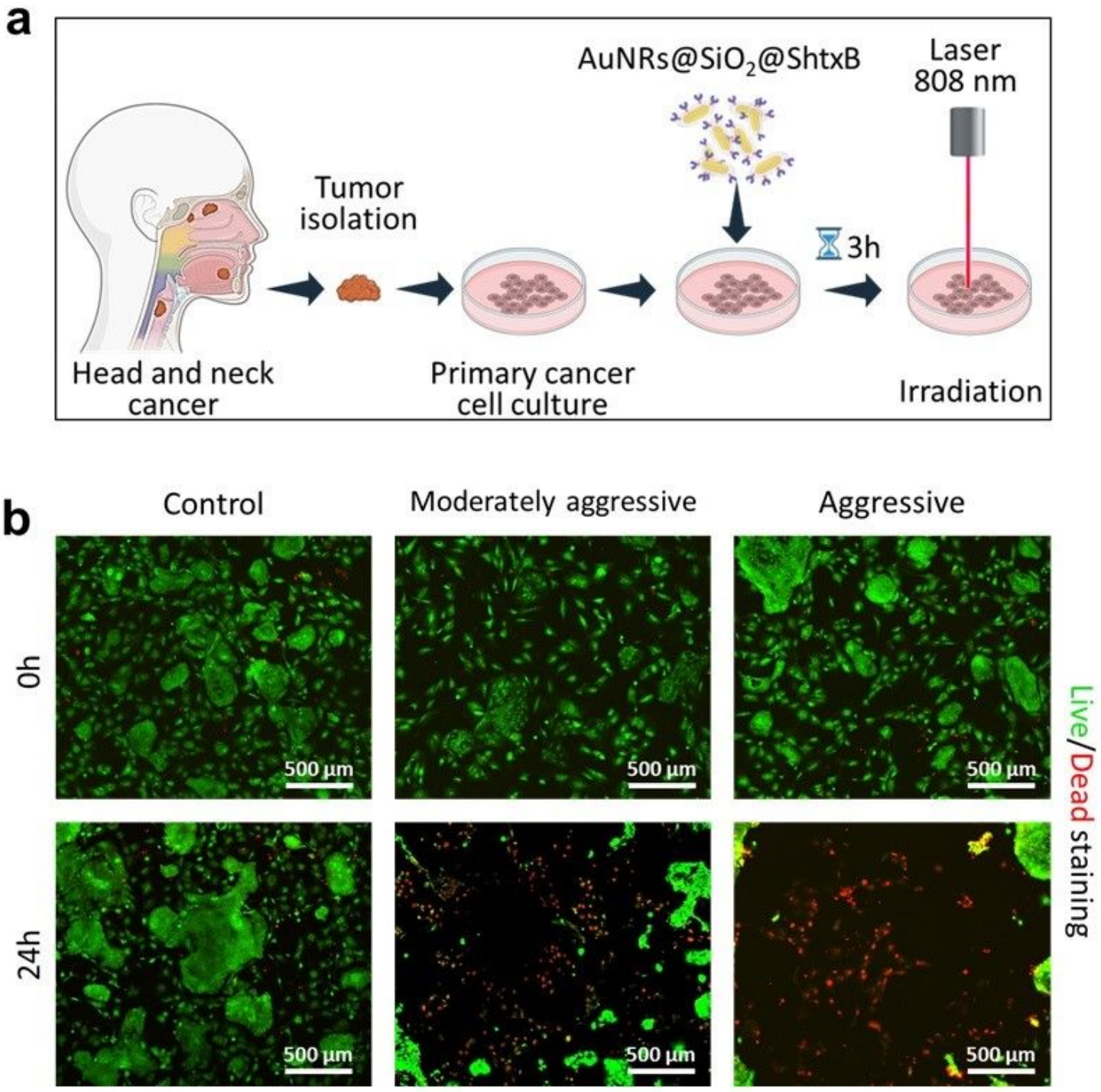

Figure 7

(a) Diagram of the experimental procedure for obtaining biopsy sample cell cultures. (b) Live/dead confocal microscopy images of biopsy cells treated with AuNRs@SiO_2@ShTxB, irradiated with a LD for 10 min and observed immediately (0h), or 24h. Both, the moderately aggressive (MASCC cells) and the aggressive squamous cell carcinoma human cells (ASCC cells) were efficiently eliminated 24 h post after 808 nm LD irradiation. In both cases, the shedding of dead cells at the radiation zone is very evident. Control cells of healthy patients were not affected by the same treatment.

Supplementary Files

This is a list of supplementary files associated with this preprint. Click to download.

- Navarro.PetalSI.pdf
- floatimage1.png